ELSEVIER

Soil Dynamics and Earthquake Engineering 25 (2005) 827–837

SOIL DYNAMICS AND EARTHQUAKE ENGINEERING

www.elsevier.com/locate/soildyn

# Diffraction of seismic waves in an elastic, cracked halfplane using a boundary integral formulation

A. Rodríguez-Castellanos[a], F. Luzón[b], F.J. Sánchez-Sesma[c,*]

[a]*Instituto Mexicano del Petróleo, Eje Central L. Cárdenas 152, CP 07730 México, DF, Mexico*
[b]*Departamento de Física Aplicada, Universidad de Almería, Cañada de San Urbano s/n., Almería 04120, Spain*
[c]*Instituto de Ingeniería, Universidad Nacional Autónoma de México, Ciudad Universitaria, Apdo. 70-472, CP 04510 México DF, Mexico*

Accepted 15 April 2005

**Abstract**

The presence of subsurface cracks in a halfspace excited by elastic waves may give rise to scattered body and surface waves. For many engineering applications, such as non-destructive testing or oil exploration, the scattered field may yield valuable information to detect cracks and other scatterers. We use the Indirect Boundary Element Method (IBEM) to study the diffraction of P, SV waves with various incidence angles and Rayleigh surface waves. This approximate boundary integral technique is based upon the integral representation for scattered elastic waves using single-layer boundary sources. Our approach is usually called *indirect* BEM as the sources' strengths should be obtained as an intermediate step. This indirect formulation can give to the analyst a deep physical insight on the generated diffracted waves because it is closer to the physical reality and can be regarded as a realization of Huygens' Principle. In any event, mathematically it is fully equivalent to the classical Somigliana's representation theorem. In order to gauge accuracy we test our method by comparing with previous results in the literature. Various crack configurations, including multiple cracks, are investigated. Results in frequency and time domains are displayed. Under certain conditions the amplitude spectra of those waves clearly show conspicuous resonance peaks.


*Keywords:* Wave propagation; Rayleigh waves; Diffraction; Crack

## 1. Introduction

The presence of cracks in structural elements or mechanical components is relatively frequent in several industrial facilities. Such cracks are caused by excessive loads, fatigue of the material and inherent defects related to both production and installation processes. These irregularities cause enormous concerns to the engineers of the structural and mechanics area. The common tools of the Resistance of Materials [1] are insufficient to study in detail the behavior of cracked media. The use of the approaches developed in Fracture Mechanics is required.

The fundamental ideas on the cracked solid behavior are due to the pioneering work by Griffith [2] who introduced them by means of an energy criterion. Years later Irwin [3] and Orowan [4] settled down the bases to incorporate the fracture mechanics as an engineering discipline. At the same time concepts like wave propagation velocities in solids, evaluation of the kinetic energy in a cracked body and crack propagation velocity limits were introduced to fracture mechanics, by Mott [5], Roberts and Wells [6] and Stroh [7], respectively. With those concepts the treatment of problems related with the dynamic effects in cracked solids began to appear establishing the bases of the Fracture Dynamics.

An important contribution was carried out by Yoffé [8] who determined the stress field at the vicinity of a crack tip propagating in an infinite region. Other investigators as Craggs [9], Broberg [10], Baker [11] and Freund [12] studied the crack curving, crack branching and crack arrest problems, besides wave diffraction in solids due to the presence of stationary or propagating cracks.

Achenbach et al. [13,14] studied the scattering of ultrasonic waves by cracks that are located at or near the free surface of an elastic body. Incident longitudinal and transverse body waves as well as Rayleigh surface waves

* Corresponding author. Tel.: +52 5 6 223 465; fax: +52 5 6 161 514.
*E-mail addresses:* arcastel@imp.mx (A. Rodríguez-Castellanos), fluzon@ual.es (F. Luzón), sesma@servidor.unam.mx (F.J. Sánchez-Sesma).

0267-7261/$ - see front matter © 2005 Elsevier Ltd. All rights reserved.
doi:10.1016/j.soildyn.2005.04.009

were considered. A horizontal subsurface crack subjected to time harmonic excitation was analyzed by Keer et al. [15].

Numerical methods have been developed for the solution of problems in fracture dynamics and specifically for those related with the interaction of waves in cracked media. Such techniques have been good to simulate components or cracked systems subject to different load and boundary conditions. One of these numerical methods is the Finite Difference Method that has been applied to solve wave propagation problems in cracked media [16].

At the beginning of the 1990s an indirect formulation of boundary elements was developed to deal with problems related to ground motion analysis, which has been successfully applied to evaluate the incidence of P, SV and Rayleigh waves on both 2D and 3D topographies [17–21]. A special case of indirect formulations was proposed by Croch [22], Siebrits and Crouch [23] and Shou et al. [24], where the solution of elastodynamic and elastostatic problems was done by placing $N$ discontinuities of unknown magnitude along the boundaries of the region to be studied, then setting up and solving a system of algebraic equations to find the unknown values that produce the specified boundary conditions. These methods are considered in the extensive review of boundary elements formulations for elastodynamic problems done by Beskos [25], in which several methodologies to study the diffraction of elastic waves by surface and subsurface cracks were pointed out. This review includes direct formulations and non-conventional ones, considering indirect formulations, applied to media excited by dynamic loads.

Boundary integral formulations have been applied to a wide range of problems with cracks, even those related with wave propagation phenomena [26]. The most important parameter to be evaluated in dynamic fracture mechanic problems is the Stress Intensity Factor (SIF). For the computation of the dynamic SIF in a halfspace and finite body loaded by steady state waves Chirino and Dominguez [27] used traction singular quarter-point boundary elements. Their method was applied to study resonance effects due to a crack located near a free surface and was compared with results published by Keer et al. [15].

To evaluate the asymptotic behavior of displacements and tractions near the crack tip by means of direct BEM in elastic wave scattering it has been necessary to deal with hypersingular integrals [28–31]. The symmetric Galerkin Boundary Element Method was developed by Bonnet et al. [32], where the symmetry was used to solve dynamic problems in fracture mechanics.

Several techniques to obtain the SIF by BEM have been developed. For instance, the multiregion method, quarter-point elements, path-independent contour integrals, energy methods, subtraction of singularity method and the weight function methods [33]. Dual formulations have been also studied in problems when hypersingular integral are present [34]. A review of SIF evaluation and modeling of singularities in BEM was done by Mukhopadhyay et al. [35], where several cases to illustrate the evaluation of the SIF are included.

More recently, scattering of seismic waves by cracks in multi-layered geological regions has been studied by means of a hybrid boundary integral equation method. Internal and interface cracks are considered and the influence of various key parameters of the problem on the scattered displacement field and on the SIF are evinced [36–39].

In this work an approximate boundary integral formulation is proposed to study the diffraction of elastic waves by subsurface cracks in an elastic halfspace. We are aware the scattering of elastic waves by cracks using the direct BEM leads to hypersingular integrals when boundary conditions are enforced. In fact, we just mentioned above a number of pioneering works on the subject. However, such approaches require considerable mathematical skills. We wanted to keep the formulation simple, as simple as the indirect BEM. To this end we used the multiregion concept, an idea used with success in the past [33], and restrict ourselves to work with single-layer boundary integrals. In our indirect approach the emphasis is laid on the scattered field rather than on the accurate evaluation of SIF for crack stability or crack growth assessment. This is beyond the scope of the present treatment. It can be done with IBEM but requires further scrutiny.

In what follows the IBEM is briefly reviewed and the integral representation is given using the Green's function for an unbounded space. Cracks are introduced at the interface of a virtual layer in which the boundary conditions (of zero tractions at crack's faces and continuity of displacements and tractions at the connecting segments) lead to a linear system of equations. This approach is validated by comparison of results for a horizontal subsurface crack reported in the literature [13] with very good agreement. Several examples are presented. They show the goodness of this method to generate valuable insight on the response of a cracked solid.

Our integral formulation can be extended to problems with multiple layers with several cracks and more complex geometries. In this case the size of the system of integral equation could be very large [26,33] and recursive techniques using reflection/transmission coefficients are in order [40].

## 2. Integral representation

Consider a domain $V$, bounded by surface $S$. If this domain is occupied by an elastic material, the displacement field under harmonic excitation can be written, neglecting body forces, by means of the single-layer boundary integral equation

$$u_i(\mathbf{x}) = \int_S \phi_j(\xi) G_{ij}(\mathbf{x};\xi)\mathrm{d}S_\xi, \tag{1}$$

where $u_i(\mathbf{x}) = i$th component of the displacement at point $\mathbf{x}$, $G_{ij}(\mathbf{x};\xi)$, Green's function, which is the displacement produced

in the direction $i$ at $\mathbf{x}$ due to the application of a unit force in direction $j$ at point $\boldsymbol{\xi}$, $\phi_j(\boldsymbol{\xi})$ is the force density in the direction $j$ at point $\boldsymbol{\xi}$. The product $\phi_j(\boldsymbol{\xi})\mathrm{d}S_{\boldsymbol{\xi}}$ represents a distribution of forces at the surface $S$ (the subscripts $i,j$ are restricted to be 1 or 3 and the summation convention is applied, i.e. a repeated subscript implies summation over its range, 1 and 3 in this case). The subscript in the differential shows the variable over which the integration is carried out. This integral representation can be obtained from Somigliana's identity [17]. Moreover, it was proved that if $\phi_j(\boldsymbol{\xi})$ is continuous *along* $S$, then the displacements field is continuous *across* $S$ [41].

This integral representation allows the calculation of stresses and tractions by means of the direct application of Hooke's law and Cauchy's equation, respectively, except at boundary singularities, that is, when $\mathbf{x}$ is equal to $\boldsymbol{\xi}$ on surface $S$. From a limiting process based on equilibrium considerations around an internal neighborhood of the boundary, it is possible to write, for $\mathbf{x}$ on $S$

$$t_i(\mathbf{x}) = c\phi_i(\mathbf{x}) + \int_S \phi_j(\boldsymbol{\xi}) T_{ij}(\mathbf{x};\boldsymbol{\xi})\mathrm{d}S_{\boldsymbol{\xi}}, \tag{2}$$

where $t_i(\mathbf{x})$ is the $i$th component of traction, $c=0.5$ if $\mathbf{x}$ tends to the boundary $S$ 'from inside' the region, $c=-0.5$ if $\mathbf{x}$ tends $S$ 'from outside' the region, or $c=0$ if $\mathbf{x}$ is not at $S$. $T_{ij}(\mathbf{x};\boldsymbol{\xi})$ is the traction Green's function, that is to say, the traction in the direction $i$ at a point $\mathbf{x}$, associated to the unit vector $n_i(\mathbf{x})$, due to the application of a unit force in the direction $j$ at $\boldsymbol{\xi}$ on $S$.

## 3. Two-dimensional Green's functions in unbounded space

In a homogeneous isotropic elastic unbounded medium, the 2D Green's functions are the responses of the medium (displacements and tractions, respectively) at a given location $\mathbf{x}$ when a unit line load is applied at $\boldsymbol{\xi}$. In what follows the expressions given in [17] are summarized.

Assuming harmonic time dependence $\exp(\mathrm{i}\omega t)$, where $\mathrm{i}=\sqrt{-1}$; $\omega$, circular frequency, and $t$, time, the displacement in the direction $i$ when the load is applied in the direction $j$ can be expressed as:

$$G_{ij}(\mathbf{x};\boldsymbol{\xi}) = A\delta_{ij} - B(2\gamma_i\gamma_j - \delta_{ij}). \tag{3}$$

On the other hand, the tractions at $\mathbf{x}$ in direction $i$ for a given unit vector $n_i$ normal to $S$ when the unit load is applied at $\boldsymbol{\xi}$ in the direction $j$ are:

$$T_{ij} = \frac{\mu}{r}\left\{\left[-4B + \lambda\frac{D(\omega r/\alpha)}{2\mu\alpha^2}\right]\gamma_j n_i + \left[-4B + \frac{D(\omega r/\beta)}{2\beta^2}\right]\times[\gamma_i n_j + \gamma_k n_k \delta_{ij}]\right\} + \frac{\mu}{r}\{(C+16B)\gamma_i\gamma_j\gamma_k n_k\}. \tag{4}$$

For Eqs. (3) and (4) we define

$$A = \frac{1}{\mathrm{i}8\rho}\left[\frac{H_0^{(2)}(\omega r/\alpha)}{\alpha^2} + \frac{H_0^{(2)}(\omega r/\beta)}{\beta^2}\right], \tag{5}$$

$$B = \frac{1}{\mathrm{i}8\rho}\left[\frac{H_2^{(2)}(\omega r/\alpha)}{\alpha^2} - \frac{H_2^{(2)}(\omega r/\beta)}{\beta^2}\right], \tag{6}$$

$$C = \frac{D(\omega r/\alpha)}{\alpha^2} - \frac{D(\omega r/\beta)}{\beta^2}, \tag{7}$$

$$D(p) = \frac{\mathrm{i}}{2\rho}pH_1^{(2)}(p), \tag{8}$$

where $\lambda$ and $\mu$ are the Lamé's constants; $\rho$, mass density; $\alpha=\sqrt{(\lambda+2\mu)/\rho}$ and $\beta=\sqrt{\mu/\rho}$ are the P and S wave velocities, respectively, $r=\sqrt{(x_1-\xi_1)^2+(x_3-\xi_3)^2}$, $\gamma_j=(x_j-\xi_j)/r$; $\delta_{ij}$, Kronecker's delta ($=1$ if $i=j$, $=0$ if $i\neq j$) and $H_m^{(2)}(\cdot)$ is the Hankel's function of second kind and order $m$.

## 4. Formulation of the problem

Starting from the configuration shown in Fig. 1, it is convenient to divide the domain in two regions ($R$ and $E$), in which adequate boundary conditions that represent the

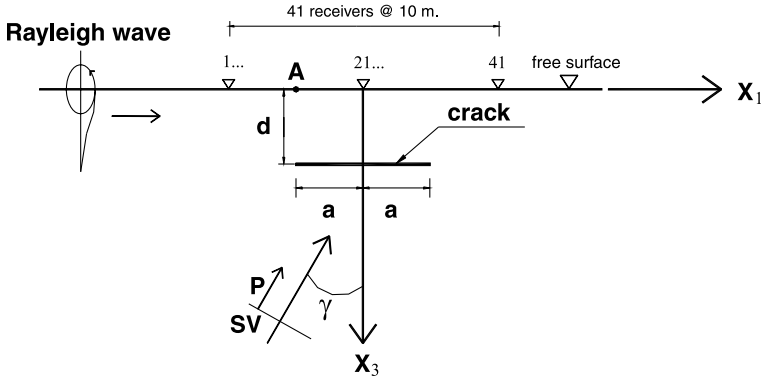


Fig. 1. Elastic halfspace that contains a crack and incidence of P, SV and Rayleigh waves.

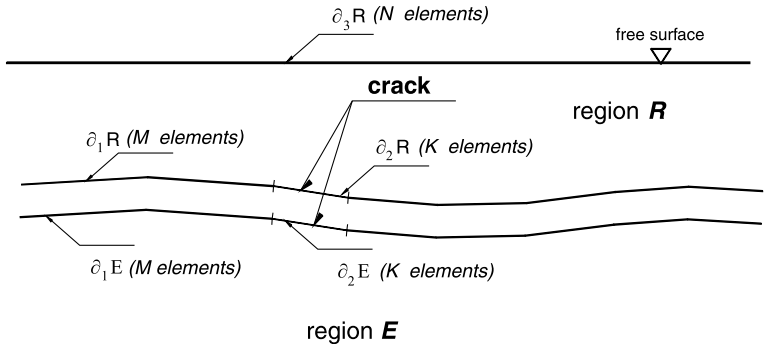


Fig. 2. Regions $R$ and $E$ of the elastic halfspace. The free surface is discretized into $N$ elements, the crack into $K$ elements, and the common interface among $R$ and $E$ into $M$ elements.

problem considered have to be established. Fig. 2 shows the configuration for regions where the boundaries of the domain are: $\partial R = \partial_1 R \cup \partial_2 R \cup \partial_3 R$ for region $R$ and $\partial E = \partial_1 E \cup \partial_2 E$ for region $E$.

### 4.1. Boundary conditions

According to Fig. 2 traction-free boundary condition is reached at the free surface ($\partial_3 R$), then this can be represented by writing

$$t_i^R(\mathbf{x}) = 0, \quad \mathbf{x} \in \partial_3 R. \tag{9}$$

On the other hand, at the common interface between region $R$ and $E$, the continuity of displacements and tractions is given as

$$u_i^R(\mathbf{x}) = u_i^E(\mathbf{x}), \quad \mathbf{x} \in \partial_1 R = \partial_1 E, \tag{10}$$

$$t_i^R(\mathbf{x}) = t_i^E(\mathbf{x}), \quad \mathbf{x} \in \partial_1 R = \partial_1 E. \tag{11}$$

Also, along the crack the tractions are null and therefore we have

$$t_i^E(\mathbf{x}) = 0, \quad \mathbf{x} \in \partial_2 E, \tag{12}$$

and

$$t_i^R(\mathbf{x}) = 0, \quad \mathbf{x} \in \partial_2 R. \tag{13}$$

Considering that both tractions and displacements on each region $E$ and $R$ can be expressed as the contribution of the free-field (the analytic solution of the halfspace without cracks) and the diffracted field, then the Eqs. (9)–(13) can be written as

$$t_i^R(\mathbf{x}) = t_i^{0^R}(\mathbf{x}) + t_i^{d^R}(\mathbf{x}) = 0, \quad \mathbf{x} \in \partial_3 R, \tag{14}$$

$$u_i^{d^R}(\mathbf{x}) + u_i^{0^R}(\mathbf{x}) = u_i^{d^E}(\mathbf{x}) + u_i^{0^E}(\mathbf{x}), \quad \mathbf{x} \in \partial_1 R = \partial_1 E, \tag{15}$$

$$t_i^{d^R}(\mathbf{x}) + t_i^{0^R}(\mathbf{x}) = t_i^{d^E}(\mathbf{x}) + t_i^{0^E}(\mathbf{x}), \quad \mathbf{x} \in \partial_1 R = \partial_1 E, \tag{16}$$

$$t_i^E(\mathbf{x}) = t_i^{0^E}(\mathbf{x}) + t_i^{d^E}(\mathbf{x}) = 0, \quad \mathbf{x} \in \partial_2 E, \tag{17}$$

and

$$t_i^R(\mathbf{x}) = t_i^{0^R}(\mathbf{x}) + t_i^{d^R}(\mathbf{x}) = 0, \quad \mathbf{x} \in \partial_2 R, \tag{18}$$

respectively. The super-index 0 stands for the free field, and $d$ for the diffracted one. Now, using the integral representations of Eq. (1) for displacements and (2) for tractions, Eqs. (14)–(18) can be expressed as

$$c\phi_i^R(\mathbf{x}) + \int_{\partial R} \phi_j^R(\boldsymbol{\xi}) T_{ij}^R(\mathbf{x};\boldsymbol{\xi}) \mathrm{d}S_\xi = -t_i^{0^R}(\mathbf{x}), \quad \mathbf{x} \in \partial_3 R, \tag{19}$$

$$\int_{\partial R} \phi_j^R(\boldsymbol{\xi}) G_{ij}^R(\mathbf{x};\boldsymbol{\xi}) \mathrm{d}S_\xi - \int_{\partial E} \phi_j^E(\boldsymbol{\xi}) G_{ij}^E(\mathbf{x};\boldsymbol{\xi}) \mathrm{d}S_\xi = u_i^{0^E}(\mathbf{x}) - u_i^{0^R}(\mathbf{x}), \quad \mathbf{x} \in \partial_1 R = \partial_1 E, \tag{20}$$

$$c\phi_i^R(\mathbf{x}) + \int_{\partial R} \phi_j^R(\boldsymbol{\xi}) T_{ij}^R(\mathbf{x};\boldsymbol{\xi}) \mathrm{d}S_\xi - c\phi_i^E(\mathbf{x}) - \int_{\partial E} \phi_j^E(\boldsymbol{\xi}) T_{ij}^E(\mathbf{x};\boldsymbol{\xi}) \mathrm{d}S_\xi = t_i^{0^E}(\mathbf{x}) - t_i^{0^R}(\mathbf{x}), \quad \mathbf{x} \in \partial_1 R = \partial_1 E, \tag{21}$$

$$c\phi_i^E(\mathbf{x}) + \int_{\partial E} \phi_j^E(\boldsymbol{\xi}) T_{ij}^E(\mathbf{x};\boldsymbol{\xi}) \mathrm{d}S_\xi = -t_i^{0^E}(\mathbf{x}), \quad \mathbf{x} \in \partial_2 E, \tag{22}$$

and

$$c\phi_i^R(\mathbf{x}) + \int_{\partial R} \phi_j^R(\boldsymbol{\xi}) T_{ij}^R(\mathbf{x};\boldsymbol{\xi}) \mathrm{d}S_\xi = -t_i^{0^R}(\mathbf{x}), \quad \mathbf{x} \in \partial_2 R, \tag{23}$$

respectively. In order to solve numerically the system of integral equations formed by Eqs. (19)–(23) we have to discretize them.

### 4.2. Discretization

In this section we present an example of discretization choosing the Eqs. (19) and (20). In these equations the integral for tractions and displacements have to be performed. Assuming that force densities $\phi_j$ are constant on each of the elements that form the surfaces of regions $E$ and $R$ (see Fig. 2), Eq. (19) can be written as

$$\sum_{p=1}^{N+M+K} \phi_j^R(\xi_p) t_{ij}^R(\mathbf{x}_q;\xi_p) = -t_i^{0^R}(\mathbf{x}_q), \quad q = 1,\ldots,N, \tag{24}$$

where

$$t_{ij}^R(\mathbf{x}_q;\xi_p) = (\pm)\frac{1}{2}\delta_{ij}\delta_{qp} + \int_{\Delta S_p} T_{ij}^R(\mathbf{x}_q;\xi)\mathrm{d}S_\xi. \tag{25}$$

The use of constant $\phi_j$ on each boundary element is enough to study the elastic waves diffracted by subsurface cracks. The crack tip stress concentrations, which are very important in fracture mechanics, reveal a local effect with little influence on the waves diffracted by cracks. It can be shown that exact radiated waves depend upon an integral of the traction Green's tensor weighted by the Crack Opening Displacement (COD or displacement discontinuity) and are relatively insensitive to stress concentrations [42]. On the other hand, it is well known that crack growth produces significant radiation of high frequency waves [43]. However, this phenomenon is beyond the scope of the present treatment.

The integrals in Eq. (25) are calculated numerically with Gaussian integration using 3 points per segment except when $\mathbf{x}=\xi$, in such a case can be shown that, for straight segments as the ones used here, the integral is null, and therefore we have

$$t_{ij}^R(\mathbf{x}_q;\xi_p) = (\pm)\frac{1}{2}\delta_{ij}. \tag{26}$$

On the other hand, the discretized version of Eq. (20) can be written as

$$\sum_{p=1}^{N+M+K} \phi_j^R(\xi_p) g_{ij}^R(\mathbf{x}_q;\xi_p) - \sum_{p=1}^{M+K} \phi_j^E(\xi_p) g_{ij}^E(\mathbf{x}_q;\xi_p) = 0, \tag{27}$$

$q = 1,\ldots,M,$

where

$$g_{ij}^l(\mathbf{x}_q;\xi_p) = \int_{\Delta S_p} G_{ij}^l(\mathbf{x}_q;\xi)\mathrm{d}S_\xi,\ l = R,E. \tag{28}$$

The integrals in Eq. (28) are calculated numerically using Gaussian integration as well. Similar expressions can be derived for Eqs. (21)–(23) using the same discretization scheme presented in Eq. (24). Once the unknowns $\phi_j$ are calculated, it is possible to compute the displacement in a point using the discretized version of Eq. (1) plus the analytic free field $u^0$.

## 5. Testing of the method

In order to validate our approximate method we took the results obtained by Achenbach et al. [13] for a horizontal crack with a total longitude $2a$ located in a depth $d$ from the free surface. These authors studied the normal incidence of P and SV waves in a halfspace and the waves generated at the free surface that travel towards the interior of the medium. In our example we assumed the incidence of P waves and the same geometrical characteristics and elastic properties of the halfspace. Achenbach et al. [13] considered different ratios $d/2a$ with the purpose of displaying the corresponding dimensionless horizontal displacements $U_L$, versus the dimensionless frequency $\omega d/C_R$, where $C_R$ = Rayleigh's wave velocity. These authors assumed the Poisson's ratio $\nu = 0.3$, S wave velocity $\beta = 100$ m/s, four ratios $d/2a = 0.2$, 0.4, 0.6 and 1.0, and a range of dimensionless frequencies given by $0 \le \omega d/C_R \le 3.0$. The dimensionless displacements at the surface are determined by means of the following equation

$$U_L = \frac{\mu}{\lambda + 2\mu}\frac{d}{b}\frac{1}{(k_L d)\mathrm{sen}(k_L d)}\left|\frac{\boldsymbol{u}_{xs}}{F}\right|, \tag{29}$$

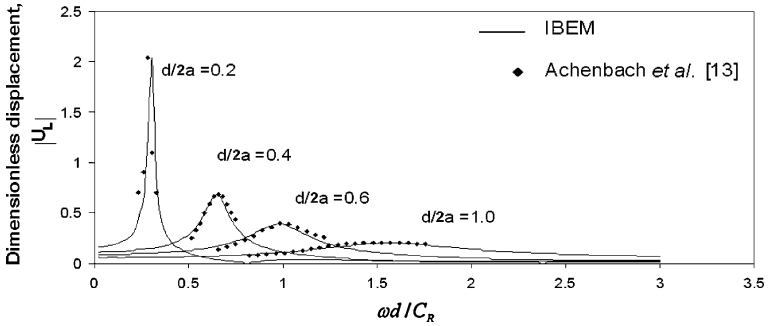


Fig. 3. Dimensionless displacements $U_L$ for the model of Fig. 1 (see text for details). The curves with continuous line represent the results obtained by our method, the diamond symbols represent results obtained by Achenbach et al. [13].

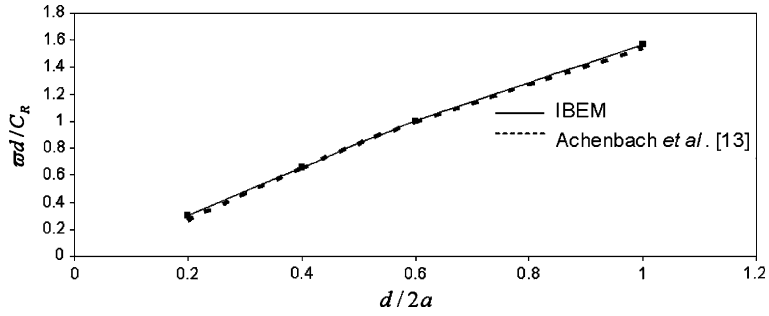


Fig. 4. Curve that relates resonant frequency $\omega d/C_R$ and $d/2a$. The curve with continuous line represents the results obtained by our method, the curve with dashed line represents those obtained by Achenbach et al. [13].

where $\boldsymbol{u}_{xs}$ is the displacement that can be computed by means of our IBEM code; in this case we compute this displacement for incident P waves. Also, $b=2a$, $k_L=$wave number defined by $k_L=\omega/a$, $F=$factor that depends on the ratio $d/2a$, and $\omega$, $\alpha$, $\mu$ y $\lambda$ were defined previously. Eq. (29) was obtained by Achenbach et al. [13] and is used here to obtain surface dimensionless displacements in the same way.

Fig. 3 display the dimensionless displacements at point $A$ for the ratios $d/2a=0.2$ 0.4, 0.6 and 1.0. The curves show different peaks, which are associated to resonances of the layer located between the up crack face and the free surface. This resonant frequency corresponds to the fundamental frequency for each case $d/2a$. For the smallest ratio ($d/2a=0.2$) it is observed that the resonance peak is the largest and corresponds to the most flexible layer because the small dimension of $d$ in comparison with the other cases. As the ratio $d/2a$ increases (e.g. for $d/2a=1.0$) the peaks become less sharp and therefore it is more difficult to determine their resonant frequency. In Fig. 4 the dimensionless resonance frequencies ($\omega d/C_R$) versus the ratios $d/2a$ are plotted. It is remarkable the good agreement between the results obtained by Achenbach et al. [13] and those calculated with our integral formulation for all ratios $d/2a$. Curves similar to those depicted in Fig. 3, for the case of dynamic SIF computation can be seen in Keer et al. [15], Chirino and Dominguez [27] and Dominguez [29], where resonance effects can be also observed. Additional results of displacement field due to subsurface cracks can be seen in Manolis and Beskos [44].

Seventy-six boundary elements were used in the validation of the first ratio $d/2a$ ($K=20$, $M=20$ and $N=36$, for the other cases less boundary elements were necessary). For all calculations we have used 6 boundary

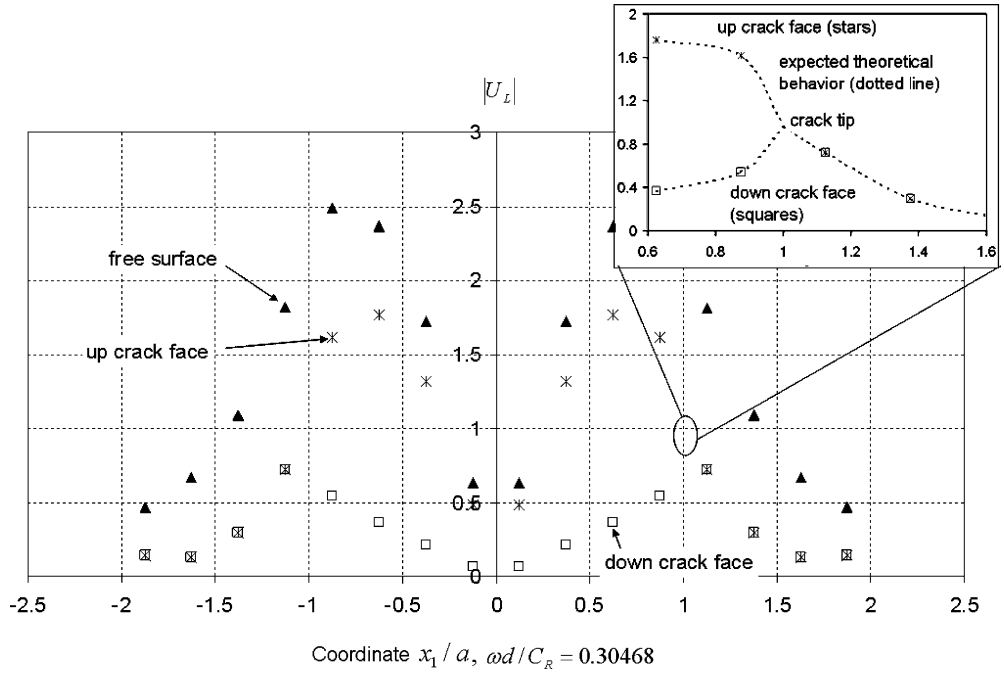


Fig. 5. Dimensionless horizontal displacements $U_L$ for collocation points at free surface, up, and down crack faces which are marked with triangles, stars and squares, respectively. The dimensionless frequency assumed is $\omega d/C_R=0.30468$. The expected theoretical variations at the crack tip zone are displayed in the figure's inset.

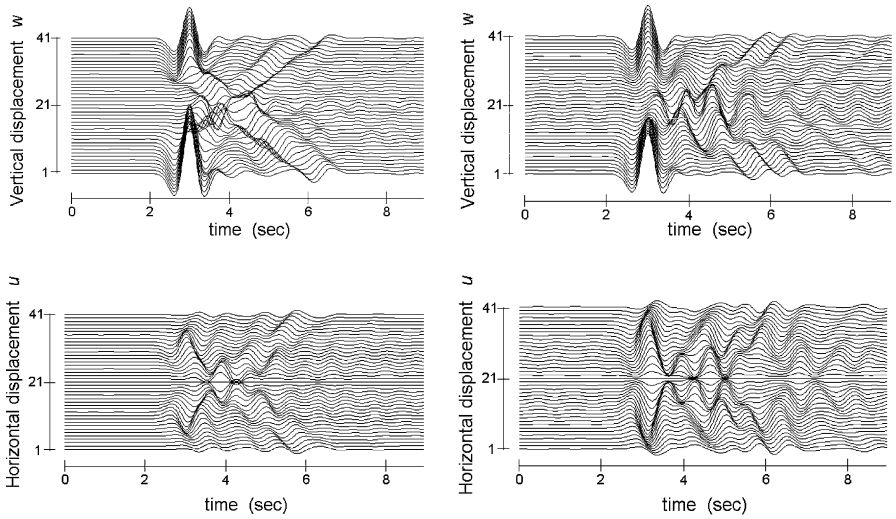


Fig. 6. Synthetic seismograms for the horizontal crack shown in Fig. 1 for normal incidence of P waves. Vertical and horizontal displacements are plotted (top and bottom, respectively), for two ratios $d/2a=0.2$ (left side) and $d/2a=0.4$ (right side).

elements per minimum wavelength and within each element Gaussian integration of three points is used. These criteria guarantee accuracy in the computations.

The displayed results (Figs. 3 and 4) correspond exclusively to the point $A$ of Fig. 1. Using our IBEM code it is possible to obtain the dimensionless displacements $U_L$ at any point of the studied model. Fig. 5 shows the dimensionless displacements $U_L$ for receivers located at the free surface, up and down crack faces. The points chosen correspond precisely to the collocation points (if fields are evaluated in other locations some mismatch may occur which is controlled by the discretization size). The dimensionless frequency $\omega d/C_R=0.30468$ corresponds to the more conspicuous peak in Fig. 3. For this frequency various peaks in the spatial distributions are observed as well. Two of them are at the free surface. This problem presents symmetry regarding the $x_3$ axis due to the geometry of the crack and the normal incidence of the P wave. The largest displacements occurs at the free surface and at distances smaller than $\pm a$. We choose this resonant frequency to display critical displacements at surface and at the crack interface. From the computed values we can extrapolate the normalized displacement at the crack tip: From the continuous portion outside the crack, the best polynomial fit leads to $U_L=0.96$ which corresponds to the average value for the up and down parts (1.26 and 0.65, respectively) of the continuous portion. The assumed constant force densities at each element (with size $\Delta S\sim 0.16\,a$) do not allow us to resolve the precise variations of stresses and displacements near the crack tip. Fortunately, the effect on diffracted waves is small and have a negligible effect on surface response, particularly for non-growing cracks. In order to increase accuracy at the crack tip some strategies already studied in the DBEM should be

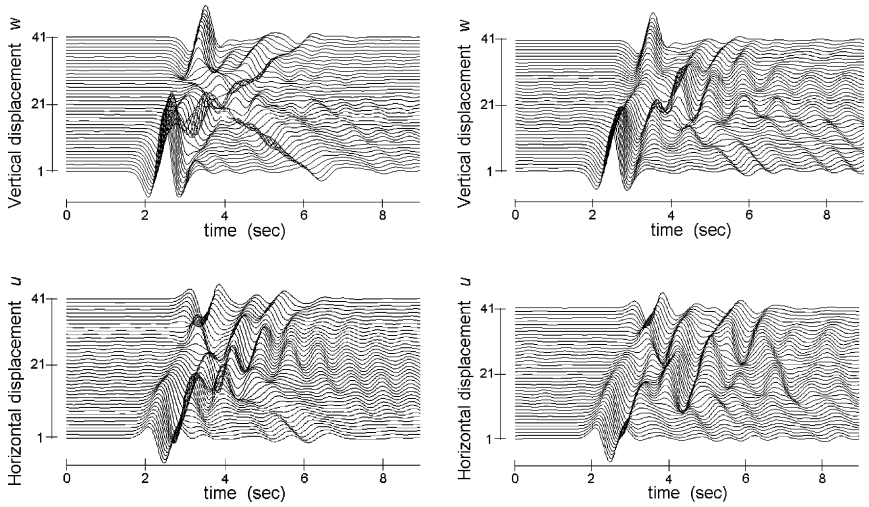


Fig. 7. Same as in Fig. 6 but for oblique incidence of P waves ($\gamma=30^\circ$).

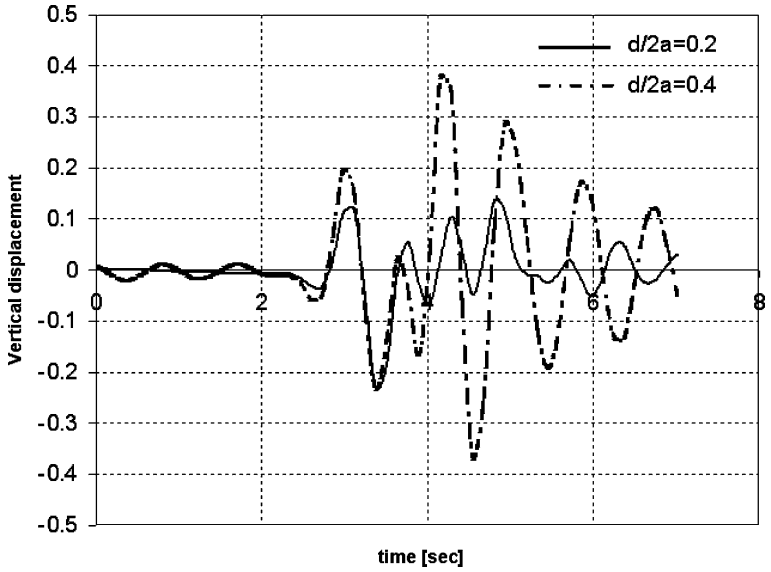


Fig. 8. Synthetic seismograms at the central receiver (number 21) for a horizontal crack as shown in Fig. 1. Vertical displacements are plotted for two ratios $d/2a=0.2$ and $d/2a=0.4$, oblique incidence of P waves ($\gamma=30°$).

implemented [15,27,29,44]. This is the subject of our current research.

## 6. Numerical examples

In this section various examples of wave propagation on medium with cracks are analyzed. We use incident P, SV and surface Rayleigh waves and compute the horizontal ($u$) and vertical ($w$) displacements. We consider two cases in the geometry of the cracks: $d/2a=0.2$ and 0.4, where $a=100$ m in both cases. We assume P and SV plane waves with incident angles of $\gamma=0°$ and 30°, with respect to the vertical. The S wave velocity is $\beta=100$ m/s, and the Poisson's ratio is $\nu=0.3$, whereas the mass density is $\rho=1$ g/cm$^3$. The quality factor considered was $Q=50$ for the propagation of both P and SV waves.

We computed, in the frequency domain, the displacements for 64 frequencies up to 3.848 Hz at various surface receivers. In order to simulate the motion along time we used the FFT algorithm to calculate synthetic seismograms using a Ricker wavelet. This pulse has a temporal dependence given by

$$R(t)=\left(a(t)-\frac{1}{2}\right)\mathrm{e}^{-a(t)}, \tag{30}$$

where

$$a(t)=\left(\frac{\pi(t-t_s)}{t_p}\right)^2, \tag{31}$$

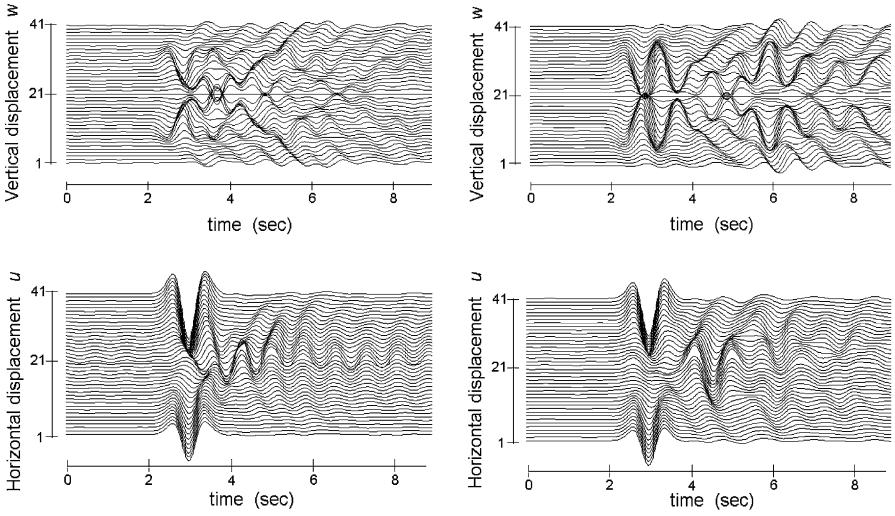


Fig. 9. Same as in Fig. 6 but for normal incidence of SV waves.

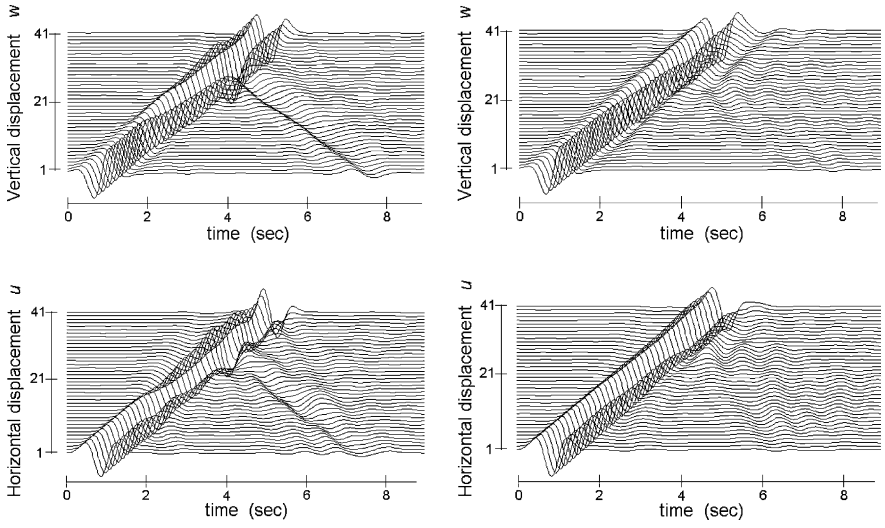


Fig. 10. Same as in Fig. 6 but for incidence of Rayleigh waves.

$t_p$, characteristic period and $t_s$, time-lag or offset. In our computations we used $t_p=1$ s and $t_s=3$ s. Figs. 6 and 7 display the synthetic displacements for P waves with incident angles of $\gamma=0$ and 30°, respectively, at 41 surface receivers located from $x_1=-200$ m up to $x_1=200$ m. In these pictures the vertical (up) and horizontal (down) displacements are presented for the two problems considered in which $d/2a=0.2$ (left side), and 0.4 (right side). It is clearly observed that for the normal incidence of plane P waves (Fig. 6) the vertical displacements are greater at those stations located far of the slit, when compared with the motion at the surface receivers just in the upward position of the crack. This is because the crack acts as a barrier, which does not, allows the arrival of the direct wave. The same effect is also observed for the P waves with $\gamma=30°$ (Fig. 7), for the two problems considered ($d/2a=0.2$ and 0.4), and principally when $d/2a$ is 0.2. This is due to the small distance between the free surface and the crack. For the other case $d/2a=0.4$ the incident and diffracted waves have more distance to interact with the up crack face and free surface, and therefore several wave interactions are observed. For instance, in Fig. 8 the vertical component at the twenty-one receivers for the two cases are plotted. It can be seen that the vertical component is less important for $d/2a=0.2$ than the response when $d/2a=0.4$. In this last case the crack is less effective as a barrier. The direct wave can interact more with the free surface and up crack face. For all $d/2a=0.4$ cases the same behavior can be observed for this incident pulse.

In Fig. 9 the synthetic seismograms for vertical incidence of SV waves are presented for the same crack and distribution of receivers as for the incidence of P waves. In this case the amplitudes of horizontal motion are larger than the vertical ones. As the direct wave only produces horizontal displacements, then the vertical ones correspond to the diffracted waves generated by the fissure. An important aspect is that the interaction in the crack is more complicated in the case of $d/2a=0.4$ for the incident pulse considered, and for example, the horizontal motion due to the diffraction at the central receivers is almost similar to the amplitude of the incident one.

The incidence of surface Rayleigh waves is illustrated in Fig. 10. In the left part it can be observed that in the shallower crack ($d/2a=0.2$) the interaction of the incident wave with the irregularity produces the emission of other wave that goes back in a direction opposite of the incident pulse. In the other hand, for the deeper fissure ($d/2a=0.4$), a similar wave going back is also seen, however, it has less

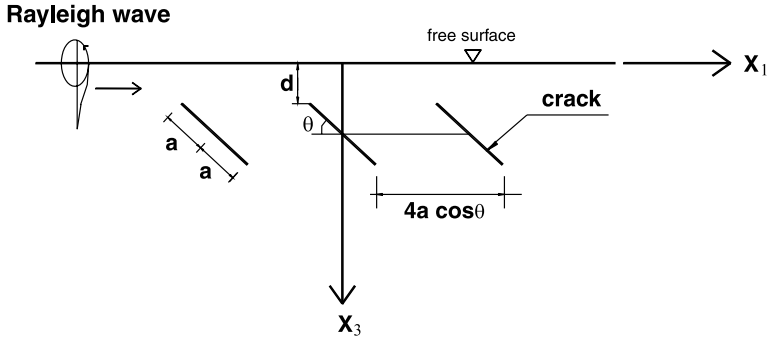


Fig. 11. Elastic halfspace containing three cracks and incidence of Rayleigh waves.

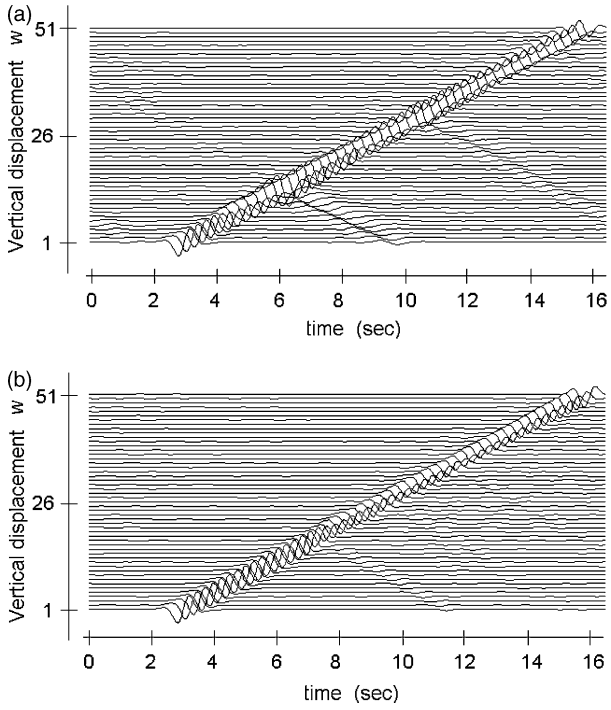


Fig. 12. Synthetic seismograms computed for the model of Fig. 11. Vertical displacements are plotted for (a) three horizontal cracks ($\theta=0°$), and (b) three cracks with angle of inclination ($\theta=60°$). Incidence of surface Rayleigh waves.

energy. This is due to the exponential decay of the incident displacements with depth, which produce less interaction of the wave with deeper cracks.

In order to observe the applicability of the method to deal with multiple cracks, we consider a model which includes various fissures, as shown in Fig. 11 with different inclination angles $\theta$. In this problem we consider the same physical properties of the medium, frequency analysis range and temporal pulse as in the previous examples, and the incidence of Rayleigh surface waves. The first case (a) corresponds to three horizontal ($\theta=0°$) cracks localized at depth $d/2a=0.2$; the second configuration (b) considers three cracks with $\theta=60°$ each one and at the depth of $d/2a=0.1$. The vertical displacements are depicted in Fig. 12 for cases (a) (up) and (b) (down) for 51 equidistant stations located on the free surface from, $x_1=-600$ m up to $x_1=600$ m. In case (a) a stronger interaction of the incident wave with the cracks can be seen. In the other (b) problem such interaction is weak. Each horizontal crack emits a backward pulse that gives rise to surface waves. Whereas the direct surface wave is traveling along the surface it is losing energy when it encounters each crack, and the waves emitted by them are each time with less amplitude. On the other hand, when the cracks have inclination they emit more diffracted energy towards the interior of the halfspace, and the generated backward waves have less amplitude (Fig. 12b) than those produced with horizontal fissures.

## 7. Concluding remarks

We applied the Indirect Boundary Element Method (IBEM) to simulate the diffraction of elastic waves within a halfspace that contains one or several cracks. The incidence of P, SV and Rayleigh waves has been considered. This numerical technique, which is based on a rigorous integral representation of the diffracted wavefield, can be seen as a realization of Huygens' Principle since the diffracted waves are constructed at the boundaries and the cracks from where they are radiated. We believe this approach can give to the analyst a deep physical insight on the generated diffracted waves because it is closer to the physical reality.

In order to validate the IBEM in the propagation of elastic waves in a cracked medium a comparison was made for a halfplane with a horizontal subsurface slit. We succeeded in reproducing results of Achenbach et al. [13]. Under certain conditions the amplitude spectra of those waves clearly show conspicuous resonant peaks. We studied the surface distribution of displacements at one of the critical resonant frequencies and found consistent spatial variations.

For the incidence of P and SV waves it has been shown that the crack behaves as a barrier for the direct waves, and at the same time produces the emission of diffracted energy which can be observed at the receivers along the free surface. Moreover, it has been observed that the crack is less effective when it is placed far from free surface and the direct P and SV waves have more distance to recover its wave front and interact with the free surface and up crack face. For the case of oblique incidence, the direct wave, reflected from the free surface, affects the trapped waves between the free surface and up crack face. For incident surface Rayleigh waves the depth and the orientation of the cracks are very important factors in the attenuation of the amplitude of the direct wave. When the slits are parallel to the free surface the backward emission of surface waves from the cracks has been observed. For inclined cracks the displacements observed at the free surface have less energy that for horizontal fissures because the greater diffracted energy towards the interior of the medium. This phenomenon may be relevant for quantitative assessment of subsurface defects.

## Acknowledgements

The comments by Prof. Dimitri Beskos and those from unknown reviewers have been crucial to improve the manuscript. The comments and suggestions of R. Avila-Carrera are greatly appreciated. This research has been partially supported by The Civil Engineering Competence of The Instituto Mexicano del Petróleo, Mexico, by CICYT, Spain, under Grants REN2002-04198-C02-02/RIES, by the European Community with FEDER, the research team RNM-194 of Junta de Andalucía, Spain, by CONACYT,

Mexico, under grant NC-204 and by DGAPA-UNAM, Mexico, under Project IN121202.

## References


[1] Timoshenko S. Strength of materials. Part I. Elementary theory and problems. 3rd ed. New York: D. Van Nostrand Company, Inc.; 1963.

[2] Griffith AA. The phenomena of rupture and flow in solids. Philos Trans R Soc London 1921;A221:163–97.

[3] Irwin GR. Fracture dynamics. In: In: Fracturing of metal. Cleveland, OH: American Society for Metals; 1948 p. 147–66.

[4] Orowan E. Fracture and strength of solids. Rep Prog Phys 1948;XII: 185.

[5] Mott NF. Fracture of metals: theoretical considerations. Engineering 1948;165:16–18.

[6] Roberts DK, Wells AA. The velocity of brittle fracture. Engineering 1954;178:820–1.

[7] Stroh AN. A theory of the fracture of metals. Adv Phys 1957;6: 418–65.

[8] Yoffé EH. The moving Griffith crack. Philos Mag 1951;42:739–50.

[9] Craggs JW. On the propagation of a crack in an elastic–brittle material. J Mech Phys Solids 1960;8:66–75.

[10] Broberg KB. The propagation of a brittle crack. Artkiv fur Fysik 1960; 18:159–92.

[11] Baker BR. Dynamic stresses created by a moving crack. J Appl Mech Trans ASME 1962;29:449–58.

[12] Freund LB. Crack propagation in an elastic solid subjected to general loading-III: stress wave loading. J Mech Phys Solids 1972;21:47–61.

[13] Achenbach JD, Lin W, Keer LM. Surface waves due to scattering by a near-surface parallel crack. IEEE Trans Son Ultrason 1983;SU-30: 270.

[14] Achenbach JD, Angel YC, Lin W. Scattering from surface-breaking and near-surface cracks. In: Johnson GC, editor. Wave propagation in homogeneous media and ultrasonic nondestructive evaluation. New York: American Society of Mechanical Engineers; 1984 [AMD 62:93].

[15] Keer LM, Lin W, Achenbach JD. Resonance effects for a crack near a free surface. J Appl Mech 1984;51:65.

[16] Chen YM. Numerical computation of dynamic stress intensity factor by a Lagrangian finite-difference method (the HEMP code). Eng Fract Mech 1975;7:653–60.

[17] Sánchez-Sesma FJ, Campillo M. Diffraction of P, SV and Rayleigh waves by topographic features; a boundary integral formulation. Bull Seismol Soc Am 1991;81:1–20.

[18] Sánchez-Sesma FJ, Ramos-Martínez J, Campillo M. An indirect boundary element methods applied to simulate the seismic response of alluvial valleys for incident P, SV and Rayleigh waves. Earthq Eng Struct Dyn 1993;22:279–95.

[19] Sánchez-Sesma FJ, Luzón F. Seismic response of three-dimensional alluvial valleys for incident P, SV and Rayleigh waves. Bull Seismol Soc Am 1995;85:269–84.

[20] Luzón F, Sánchez-Sesma FJ, Rodríguez-Zuñiga JL, Posadas AM, García JM, Martín J, et al. Diffraction of P, SV and Rayleigh waves by three-dimensional topographies. Geophys J Int 1997;129:571–8.

[21] Vai R, Castillo-Covarrubias JM, Sánchez-Sesma FJ, Komatitsch D, Vilotte JP. Elastic wave propagation in an irregularly layered medium. Soil Dyn Earthq Eng 1999;18:11–18.

[22] Crouch SL. Solution of plane elasticity problems by the displacement discontinuity method. Int J Numer Methods Eng 1976;2:301–43.

[23] Siebrits E, Crouch SL. Geotechnical applications of a two-dimensional elastodynamic displacement discontinuity method. Int J Rock Mech Min Sci Geomech Abstr 1993;30:1387–93.

[24] Shou KJ, Siebrits E, Crouch SL. Higher order displacement discontinuity method for three-dimensional elastostatic problems. Int J Rock Mech Min Sci 1997;34:317–22.

[25] Beskos DE. Boundary element methods in dynamic analysis: part II (1986–1996). Appl Mech Rev 1997;50:149–97.

[26] Zhang CH, Gross D. On wave propagation in elastic solids with cracks. Southampton: Computational Mechanics Publications; 1998.

[27] Chirino F, Dominguez J. Dynamic analysis of cracks using boundary element methods. Eng Fract Mech 1989;34:1051–61.

[28] Krishnasamy G, Schmerr LW, Rudolphi TJ, Rizzo FJ. Hypersingular boundary integral equations: Some applications in acoustic and elastic wave scattering. J Appl Mech 1990;57:404–14.

[29] Dominguez J. Boundary elements in dynamics. Southampton: Computational Mechanics Publications; 1993.

[30] Gallego R, Dominguez J. Solving transient dynamic crack problems by the hypersingular boundary element method. Fatigue Fract Eng Mater Struct 1997;20:799–812.

[31] Fedelinski P, Aliabadi MH, Rooke DP. Boundary element formulations for the dynamic analysis of cracked structures. Eng Anal Bound Elem 1996;17:45–56.

[32] Bonnet M, Maier G, Polizzotto G. Symmetric Galerkin boundary element methods. Appl Mech Rev 1998;51:669–704.

[33] Aliabadi MH. Boundary element formulations in fracture mechanics. Appl Mech Rev 1997;50:83–96.

[34] Chen JT, Hong HK. Review of dual boundary element methods with emphasis on hypersingular integrals and divergent series. Appl Mech Rev 1999;52:17–32.

[35] Mukhopadhyay NK, Maiti SK, Kakodkar A. A review of SIF evaluation and modeling of singularities in BEM. Comput Mech 2000;25:358–75.

[36] Dineva PS, Manolis GD. Scattering of seismic waves by cracks in multi-layered geological regions. I. Mechanical model. Soil Dyn Earthq Eng 2001;21:615–25.

[37] Dineva PS, Manolis GD. Scattering of seismic waves by cracks in multiple-layered geological regions. II. Numerical results. Soil Dyn Earthq Eng 2001;21:627–41.

[38] Dineva PS, Manolis GD, Rangelov TV. Transient seismic wave propagation in a multilayered cracked geological region. J Sound Vib 2004;273:1–32.

[39] Manolis GD, Dineva PS, Rangelov TV. Wave scattering by cracks in inhomogeneous continua using BIEM. Int J Solids Struct 2004;41: 3905–27.

[40] Kennett BLN. Seismic wave propagation in stratified media. Cambridge: Cambridge University Press; 1983.

[41] Kupradze VD. Dynamical problems in elasticity. In: Sneddon IN, Hill R, editors. Progress in solid mechanics, vol. III. Amsterdam: North-Holland; 1963.

[42] Sánchez-Sesma FJ, Iturrarán-Víveros U. Scattering and diffraction of SH waves by a finite crack: an analytical solution. Geophys J Int 2001; 145:749–58.

[43] Madariaga R. Dynamics of an expanding circular crack. Bull Seismol Soc Am 1976;66:639–66.

[44] Manolis GD, Beskos DE. Boundary element methods in elastodynamics. Boston, MA: Unwin-Hyman; 1988.